Precision Measurements of Correlated Energies and Velocities of ^{252}Cf Fission Fragments*

H. W. Schmitt, W. E. Kiker,† and C. W. Williams‡

Oak Ridge National Laboratory, Oak Ridge, Tennessee

(Received 9 October 1964)

Correlated energies and velocities of single fission fragments from the spontaneous fission of ^{252}Cf have been measured. Absolute energies and times of flight are obtained with estimated accuracies of ±0.5% from direct comparison measurements with 30- to 120-MeV ^{79}Br, ^{81}Br, and ^{127}I ions from the tandem Van de Graaff accelerator. The post-neutron-emission kinetic parameters obtained from this experiment for ^{252}Cf fragments are compared with pre-neutron-emission quantities obtained from double-time-of-flight experiments of Whetstone and of Milton and Fraser. Of special interest is the fine structure which appears in the post-neutron-emission mass distribution. It is shown that this structure reflects the fine structure observed in the pre-neutron-emission mass distribution, which in turn is known to reflect certain energetically preferred even-even fragment configurations in ^{252}Cf spontaneous fission. Within the ≈2.5% mass resolution of the present experiment, no additional fine structure appears as a result of neutron boil-off to specific fragment masses. The number of neutrons $\nu(M)$ as a function of fragment mass has been calculated from the pre- and post-neutron-emission mass distributions. In an appendix, a "universal" energy calibration procedure for solid-state detectors for fission fragments is given; this procedure is based on the present absolute fragment energy determinations and takes into account the mass dependence of the pulse-height-versus-energy relation.

I. INTRODUCTION

THE determinations of post-prompt-neutron-emission fission yields and mass distributions have traditionally been made by radiochemical and mass spectrometric techniques. The development of solid-state detectors, with their inherently good pulse-height resolution and fast pulse rise time, has made it attractive to determine such distributions by kinetic measurements, in particular by means of energy, time-of-flight correlation experiments. Such measurements are, however, very sensitive both to the absolute energy calibration of the solid-state detectors for fission fragments and to the absolute velocity, or time-of-flight calibration.

Accordingly, we have combined measurements on single ^{252}Cf spontaneous fission fragments with measurements on ^{79}Br, ^{81}Br, and ^{127}I ions which were accelerated in the Oak Ridge tandem Van de Graaff to energies in the 30- to 120-MeV range, to obtain precise absolute calibrations for the energy, time-of-flight correlation experiment. In the course of this experiment, new precision determinations of the kinetic parameters for ^{252}Cf fission fragments were made, and a general method for the absolute energy calibration of solid state detectors, described in Appendix II, was developed.

The mass distribution is obtained with somewhat poorer mass resolution than the radiochemical mass distribution; however, the resolution function is known, and the point-to-point uncertainties in the present experiment are smaller. New structural features, not evident in the radiochemical data, have been observed.

The measuring system, described in a previous publication,[1] included a silicon surface barrier detector for the determination of fragment energies; the detector was located at the end of a fragment flight path about two meters long. Both a linear signal, related to the fragment energy, and a timing pulse were obtained from the detector by means of a "time pickoff" scheme in which transformer coupling is employed.[2] The zero-time signal was obtained from an electron accelerating and focusing lens of the type usually used in fission fragment time-of-flight experiments.[3-5]

It is essential at the outset to distinguish clearly between the fragments before and after neutron emission. It has been shown[6] that neutrons are emitted in a time less than about 10^{-14} sec after scission, i.e., a time short compared to the flight times of the fragments which are $\gtrsim 10^{-7}$ sec in this and other experiments.[4,5,7] It is clear, therefore, that any measured kinetic parameter applies to the fragment after neutron emission. In particular, in the present experiment the measured velocities and energies are *post*-neutron-emission quantities, and the masses obtained from transformation of the data are *post*-neutron-emission masses.

In contrast, double time-of-flight experiments give information about the fragments before neutron emission,[4,5,7] as follows: It has been shown[7] that the angular

[1] C. W. Williams, W. E. Kiker, and H. W. Schmitt, Rev. Sci. Instr. 35, 1116 (1964).

[2] C. W. Williams and J. A. Biggerstaff, Nucl. Instr. Methods 25, 370 (1964).

[3] W. E. Stein and R. B. Leachman, Rev. Sci. Instr. 27, 1049 (1956).

[4] S. L. Whetstone, Jr., Phys. Rev. 131, 1232 (1963).

[5] J. S. Fraser, J. C. D. Milton, H. R. Bowman, and S. G. Thompson, Can. J. Phys. 41, 2080 (1963).

[6] J. S. Fraser, Phys. Rev. 88, 536 (1952).

[7] H. R. Bowman, J. C. D. Milton, S. G. Thompson, and W. J. Swiatecki, Phys. Rev. 129, 2133 (1963); also Phys. Rev. 126, 2120 (1962).

distributions of the neutrons are in general symmetric about 90° in the center-of-mass system of the fragment. Therefore, for a given initial fragment velocity, say v_1^*, the average final velocity (after neutron emission) is essentially equal to the initial velocity. The rigorous equation for momentum conservation, $m_1^* v_1^* = m_2^* v_2^*$ may then, on the average, be replaced by the equation $m_1^* v_1 = m_2^* v_2$, where the starred quantities are pre-neutron-emission quantities and the unstarred quantities are post-neutron-emission quantities (a notation which we shall use throughout this paper). Thus the masses and energies obtained from transformation of double time-of-flight data are essentially *pre*-neutron-emission quantities.

Comparisons of pre- and post-neutron-emission quantities are given, along with the results of cumulative yield calculations of $\nu(M^*)$, the number of neutrons emitted as a function of fragment mass.

II. METHOD AND APPARATUS

Figure 1 shows a block diagram of the energy, time-of-flight correlation system. The system design and performance have been discussed in detail previously[1] and will be described only briefly here.

The ^{252}Cf source was prepared by the self-transfer method (see Acknowledgments). The backing was 1-in.-diam, 0.005-in.-thick platinum; the deposit was ≈ 1 cm in diameter and the source activity was $\sim 3 \times 10^5$ fissions per minute.

As shown in Fig. 1, a fission fragment leaving the fissile source passed through a thin nickel foil (≈ 70 μg/cm^2) from which electrons were ejected. These elec-

trons were electrostatically accelerated and focused onto a 1.5-in.-diam, 0.002-in.-thick plastic (NE 102) scintillator which was optically coupled to an RCA 6810A photomultiplier; the accelerating voltage used on the lens was 13 kV. The current signal from the anode of the phototube was fed directly to a remotely controlled tunnel diode discriminator. The constant rise time, constant amplitude output pulse from the tunnel diode was delayed a time longer than the longest fission fragment flight time, was amplified, inverted, and fed into the "stop" side of the time-to-pulse-height converter (TPHC). Low-loss cable (Type RG 63/U, 125-Ω impedance) was used for all delays.

After passing through the nickel foil, the fission fragment moved 215.3 cm along an evacuated flight tube to a silicon surface barrier detector of about 4.5 cm^2 area. A loosely collimating set of apertures was used to prevent single-scattered and degraded fragments from reaching the detector. A rounded collimator was used at the detector to minimize tailing effects. The current pulse from the surface barrier detector passed through a transformer primary to a low noise, charge-sensitive preamplifier and then to a linear amplifier with double-delay-line shaping. The fast timing signal was taken from the transformer secondary; this signal was amplified by a voltage sensitive fast amplifier (rise time $\lesssim 3.5$ nsec) and fed into a remotely controlled tunnel diode discriminator, the output from which served as the "start" signal for the TPHC. The output from the TPHC was amplified by a double-line linear amplifier. The amplitude of this signal, along with that of the signal from the energy amplifier, was recorded on punched paper tape by a two-parameter correlation pulse-height analyzer.

In order to measure the performance of the system,[1] and in the present work to obtain absolute calibrations for the system, correlated energy, time-of-flight measurements were made on heavy ions (^{79}Br and ^{81}Br; or ^{127}I) accelerated to energies in the range 30–120 MeV by the Oak Ridge tandem Van de Graaff accelerator. Details of the production and acceleration of these ions to these energies are given in a previous publication.[8] The ions were magnetically analyzed by a 90° bending magnet yielding separated groups of particles of constant ME/q^2, or Mv/q, where M, E, and v are the ion mass, energy, and velocity, respectively, and q is the ion charge, an integral multiple of the electron charge. Typical time-of-flight spectra are shown in Ref. 1, and typical energy spectra are shown in Refs. 8 and 9. The system time resolution is ~ 2 nsec full width at half-maximum (FWHM) in the region of interest; the energy resolution was about 1.5 MeV (FWHM) and appears to be inherent in the detectors.[9] The resolution in mass was found to be 1.8 amu (FWHM) for bromine
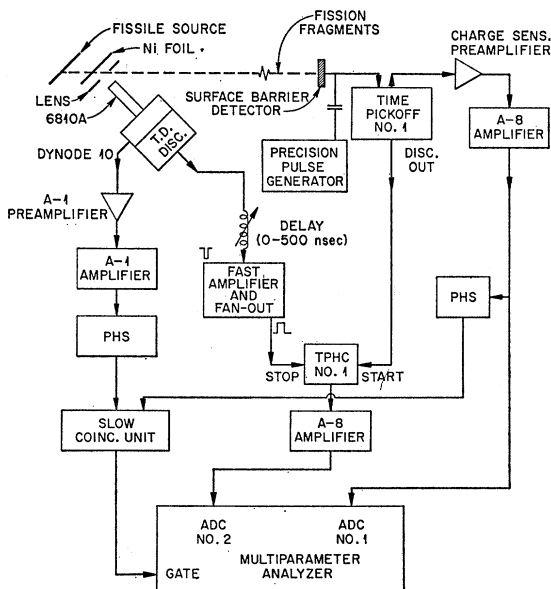

FIG. 1. Block diagram of the energy, time-of-flight correlation system, shown for fission fragment measurements. The fissile source is removed for measurements with bromine or iodine ions from the tandem Van de Graaff.

[8] C. D. Moak, J. H. Neiler, H. W. Schmitt, F. J. Walter, and G. F. Wells, Rev. Sci. Instr. 34, 853 (1963).
[9] H. W. Schmitt, W. M. Gibson, J. H. Neiler, F. J. Walter, and T. D. Thomas (to be published).
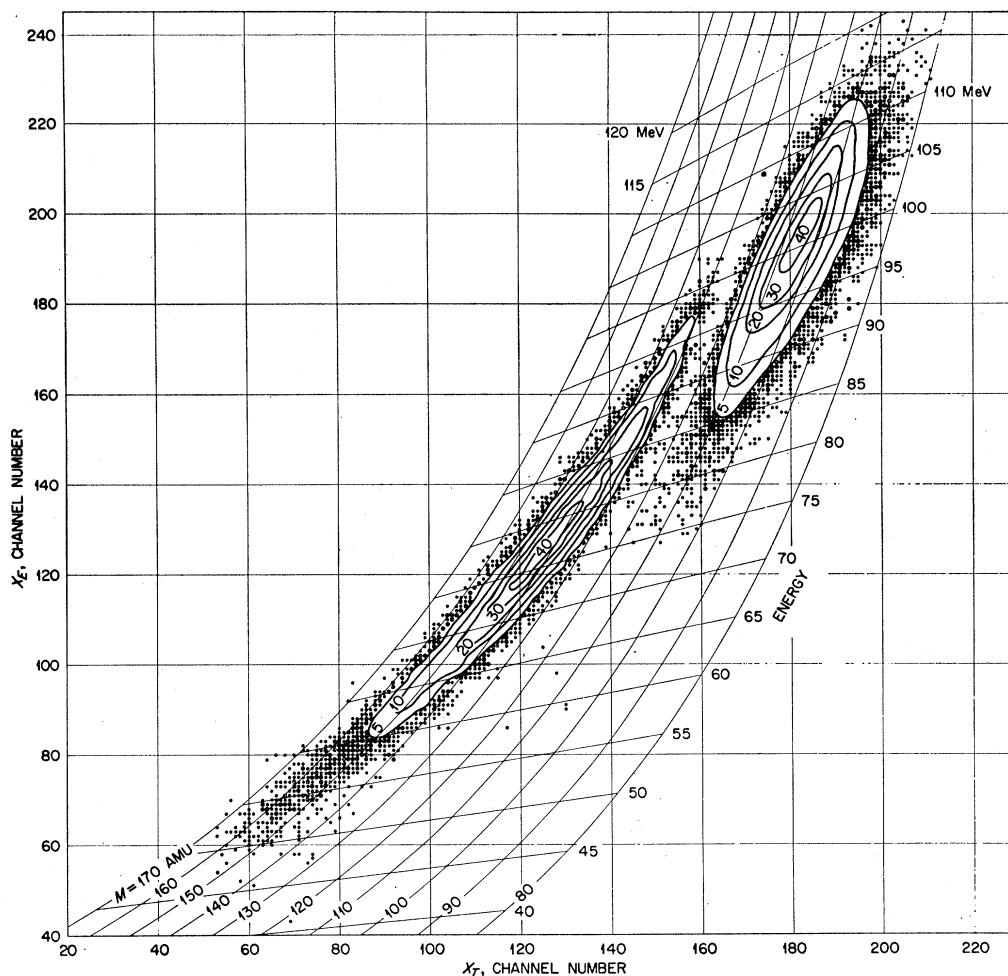
Fig. 2. Two-parameter energy, time-of-flight correlation data for ^{252}Cf spontaneous fission fragments. Flight distance $= 215.3$ cm. Numbers labeling the contours indicate the number of events per channel squared. The constant energy lines, labeled at right, are at angles to the constant pulse height (x_E) lines because of the mass dependence in the pulse-height response. Masses and energies are post-neutron-emission quantities.

ions and 3.2 amu (FWHM) for iodine ions. These subjects are discussed in detail in Refs. 1 and 9.

III. SYSTEM CALIBRATION

The determination of the absolute ion energy corresponding to each peak in a pulse-height spectrum is discussed in complete detail in Appendix I. In this section we shall discuss the calibration of the system, given that a spectrum containing discrete groups of particles of known mass and energy is available to the system.

A. Energy Calibration

The pulse-height-versus-energy relation for ions of a given mass was readily obtained. The position (channel number) for each peak was carefully located, and the pulse height was determined with reference to a precision pulse generator connected throughout the measurements as shown in Fig. 1. Typical pulse-height versus

energy curves for bromine and iodine ions are shown in Ref. 1; similar curves are presented in another context in Appendix II below. A detailed study of the pulse-height response of solid-state detectors to heavy ions is described in a separate publication.[9]

The important feature of these curves is that the relation is linear for ions of a given mass in the energy range of fission fragments. Thus

$$E = Ax + B, \qquad (1)$$

where x and E are the pulse height and ion energy, respectively, and A and B are constants for ions of a given mass. Evidence presented in Ref. 9 indicates that, in the range of masses and energies of fission fragments, the coefficient A is approximately linearly dependent on the ion mass. The value of B for iodine differs very little from that for bromine; hence, it is sufficiently accurate to introduce the assumption that B also varies linearly with ion mass. Thus we arrive at

a general form for the energy calibration of the solid-state detector for fission fragments

$$E=(a+a'M)x+b+b'M, \qquad (2)$$

where a, a', b, and b' are constants for a particular detector operated under constant conditions in the saturation region of the pulse-height versus bias curve.

In this work, the constants were readily determined from bromine and iodine runs; Eq. (2) was then used in the analysis of the energy, time-of-flight correlation data to determine fragment masses and energies. In practice, the constants may be determined in terms of channel number, provided only that the pulse analysis system is linear. Thus no reference to absolute pulse height is necessary, and the pulser points need be used only for checks of stability and linearity, and for intercalibration among successive runs.

We have included in Appendix II a general method for obtaining the four constants in Eq. (2) from a pulse-height spectrum for ^{252}Cf spontaneous fission fragments. This method should be applicable in any experiment in which solid-state detectors are used for fission fragment energy measurements.

B. Time Calibration

Calibration of the timing system is straightforward. After the pulse-height-versus-energy relation for a particular ion was obtained as described above, the thin nickel foil was inserted in the zero-time detector, care being taken to avoid other changes. A second pulse-height spectrum was obtained and, from the new pulse heights (peak locations) together with the original pulse-height-versus-energy relation, energy assignments were made for all of the peaks. From these energies, along with the known flight distance and ion mass, the ion flight times were obtained. These flight times were in turn assigned to the appropriate peaks in the time spectrum (spectrum of pulses from the time-to-pulse-height converter); thus the timing system was accurately calibrated.

It was found that time calibrations thus obtained from iodine ion measurements were in excellent agreement with those obtained from bromine measurements. Thus, no mass dependence was necessary in the time calibration equation

$$t_f=c_t+a_t x_t{}^2-b_t x_t, \qquad (3)$$

where t_f and x_t are the time-of-flight and time-pulse amplitude, respectively, and a_t, b_t, and c_t are calibration constants obtained by least-squares fit. The quadratic term in Eq. (3) was small, i.e., less than two percent in every case.

In order to provide periodic checks of the stability and linearity of the timing system, a series of delay cables (RG 63/U) were available for use as follows: A second output from the pulser, in parallel with the output shown in Fig. 2, was connected through one of

these delay lines to the fast amplifier (in place of the 0-500 nsec delay), thus providing a "stop" signal to the TPHC. The pulser connection shown in the figure supplied the "start" signal. A set of reproducible time intervals was thereby obtained; these were used for stability checks and intercalibration among successive runs in the same manner as the pulser was used in the energy spectra.

As a matter of interest, an auxiliary experiment was performed in which the relative delay times in the cables were determined by square-wave reflection and shape analysis techniques.[10] When a plot was made of ion flight time as a function of relative delay, a straight line whose slope was 1.000 ± 0.001 was obtained.

IV. DATA ANALYSIS

Correlated energy, time-of-flight data were recorded, event-by-event, on punched paper tape; 256 channels were used in each parameter. Thus the raw data of the present experiment are contained in a 256×256 channel array as shown in Fig. 2 for ^{252}Cf spontaneous fission fragments. Channels along the abscissa are related to the fragment flight time as indicated in Eq. (3); channels along the ordinate are related principally to the fragment energy, as indicated in Eq. (2).

These data have been transformed to give the mass-energy correlations and the fragment mass distribution. The transformation was accomplished as follows: Consider the x_E, x_t array of Fig. 2 described by the function $G(x_E,x_t)\Delta x_E\Delta x_t$, where Δx_E and Δx_t are each simply one channel, and $G(x_E,x_t)$ is the number of events per (channel)^2 at x_E and x_t. It follows then that

$$F(M,E)\Delta M\Delta E=G(x_E,x_t)J\begin{pmatrix}x_E & x_t\\ M & E\end{pmatrix}\Delta M\Delta E, \qquad (4)$$

where $F(M,E)$ is the number of events per unit mass and per unit energy at mass M and energy E; ΔM and ΔE are the mass and energy intervals, i.e., box sizes, chosen for the M, E array. Now consider the functions G and J.

The function $G(x_E,x_t)$ as used in Eq. (4) must be evaluated at the point x_E, x_t corresponding to the point M, E at which the value of $F(M,E)$ in the new array is desired. The point x_E, x_t, thus found from Eqs. (2) and (3), will not in general lie at integral channel numbers. Therefore, in order to evaluate the function $G(x_E,x_t)$ at nonintegral channel numbers, we have used a quadratic interpolation scheme first proposed by Thomas.[11] In this method a 3×3 submatrix is considered, with the point of interest near its center. Second-degree polynomials are fitted to values of $G(x_E,x_t)$ in each row of this submatrix, and three values are ob-

[10] The authors gratefully acknowledge the delay line measurements by W. F. Mruk.

[11] T. D. Thomas and W. M. Gibson, Proceedings of the Conference on Utilization of Multiparameter Analyzers in Nuclear Physics, Report NYO 10595, 1963 (unpublished).

tained at the correct abscissa. These values of G are then in turn fitted with a second-degree polynomial to find the value of $G(x_E, x_t)$ at the correct ordinate and abscissa.[12] The final value obtained is independent of the order of fitting, i.e., one may fit either rows or columns first with no change in the result, provided that the points are evenly spaced.

The Jacobian function J is straightforward though cumbersome to evaluate; it is given as a function of the mass and energy as follows:

$$J\begin{pmatrix} x_E & x_t \\ M & E \end{pmatrix} = \left(\frac{MD^2}{8E\{b_t^2 - 4a_t[c_t - D(M/2E)^{1/2}]\}} \right)^{1/2} \quad (5)$$

$$\times \frac{(ab' - a'b)M - aE}{EM(a + a'M)^2},$$

where D is the distance from the zero-time detector foil to the surface barrier detector.

The mass, energy array resulting from this transformation was appropriately treated to give the fragment mass distribution, the average kinetic energy as a function of fragment mass, and other parameters as discussed below. The velocity distribution was also obtained, although this distribution resulted only from a one-dimensional transformation of the time (i.e., x_t) spectrum.

V. RESULTS AND DISCUSSION

In this section we shall consider first the distributions in velocity and energy and the precise determinations of the kinetic parameters for ^{252}Cf fragments based on the heavy ion calibrations. Second, we shall consider the post-neutron-emission mass distribution, the structure which appears in it, and the neutron emission data which can be obtained from comparison with the pre-neutron-emission mass distribution.
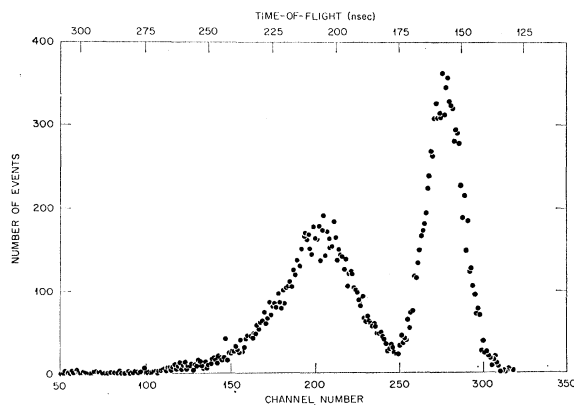
In order to obtain an absolute time-of-flight spectrum, and hence an absolute velocity spectrum for fragments unperturbed by the thin foil of the zero-time detector, a separate experiment was performed. In this experiment an absolute time calibration was obtained from heavy-ion runs as described in Sec. III. Then a fission fragment time spectrum was obtained with the ^{252}Cf source mounted directly on the electron lens, re placing the thin nickel foil (see Fig. 1). In this configuration the background in the zero-time detector was higher than normal, but was not prohibitive. Tests were made to determine the effect of the higher background in the zero-time detector; for example, data were taken at several tunnel diode discriminator levels. In addition, the present spectrum was compared in detail with one obtained with the thin nickel foil in place in the zero-time detector and the Cf source located as shown in Fig. 1. The two spectrum shapes were in excellent agreement, and the absolute differences in times were consistent with fragment energy losses in the nickel foil. The "time" pulse-height spectrum, taken in $\sim$250 channels, is shown for the unperturbed fragments in Fig. 3. The time scale was obtained from the heavy-ion calibration, and the constants in Eq. (3) were $a_t = 5.908 \times 10^{-5}$ nsec per (channel)^2, $b_t = 0.6418$ nsec per channel and $c_t = 339.17$ nsec.

The absolute velocity distribution shown in Fig. 4 was obtained from an analytical transformation of a smooth curve through the points shown in Fig. 3; thus no points are shown on this curve. For calculations

FIG. 3. Absolute time-of-flight spectrum for unperturbed ^{252}Cf spontaneous fission fragments. Flight distance=215.3 cm.

[12] This entire procedure is an approximation to a surface interpolation and seems to be adequate in this application.
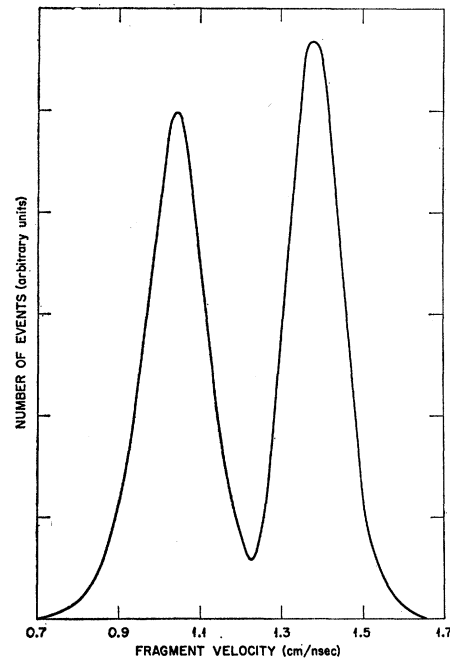

FIG. 4. Absolute velocity distribution of ^{252}Cf spontaneous fission fragments. A smooth curve drawn through the data of Fig. 5 was transformed to give the velocity distribution shown here.
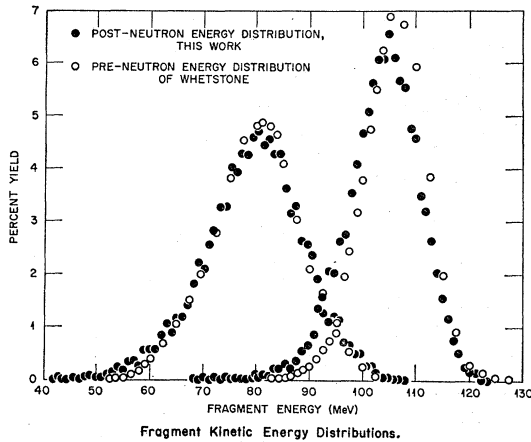
Fig. 5. Post-neutron-emission kinetic energy distributions for the light and heavy fragments from ^{252}Cf fission, compared with the pre-neutron-emission distributions of Whetstone (Ref. 4).

of $\langle v_L \rangle$ and $\langle v_H \rangle$, the average light- and heavy-fragment velocities, respectively, the shapes of the tails of the two groups in the valley were obtained from correlation data; the results were quite insensitive to these shapes. The average velocities deduced were $\langle v_L \rangle = 1.036 \pm 0.005$ cm/nsec and $\langle v_H \rangle = 1.383 \pm 0.006$ cm/nsec, where the uncertainties include those in the absolute calibration. Values of the rms width σ, where

$$\sigma^2 = \langle v^2 \rangle - \langle v \rangle^2 \qquad (6)$$

were computed for each group; the values obtained were $\sigma_{vL} = 0.0693$ cm/nsec and $\sigma_{vH} = 0.0831$ cm/nsec.

The fragment kinetic energy distribution is shown in Fig. 5. It is shown for the light- and heavy-fragment groups and was obtained from the correlation experiment. Corrections for energy loss in the foil were small, i.e., about 3 MeV,[1] and contain uncertainties of approximately ± 0.3 MeV. The pre-neutron-emission kinetic energy distribution for each group, from Whetstone,[4] is shown for comparison. The average post-neutron-emission light- and heavy-fragment kinetic energies ob-
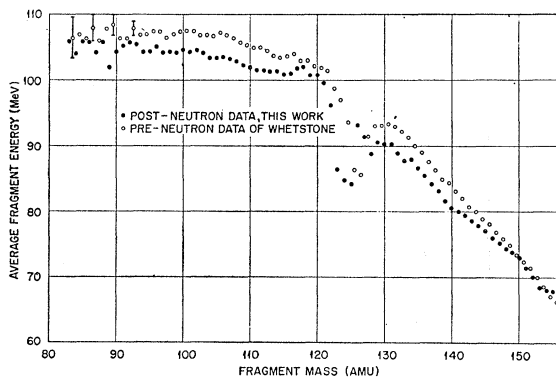
tained from the present experiment are $\langle E_L \rangle = 103.8 \pm 0.5$ MeV and $\langle E_H \rangle = 79.4 \pm 0.5$ MeV.

The average single-fragment kinetic energy is plotted as a function of fragment mass in Fig. 6. Essentially the same features are observed in the present results as are observed in those for pre-neutron-emission fragments. The dip[4] in the mass range near symmetry (~ 126 amu) is confirmed.

Table I gives a comparison of the kinetic parameters associated with ^{252}Cf spontaeous fission fragments. The average light- and heavy-fragment energies, velocities and masses are tabulated along with the values of σ for these distributions. In the table, for comparison, we also give the results of Whetstone[4] and Fraser et al.[5] It should be noted that only the fragment velocities may be compared directly among the three experiments. The agreement here is excellent. The differences be-
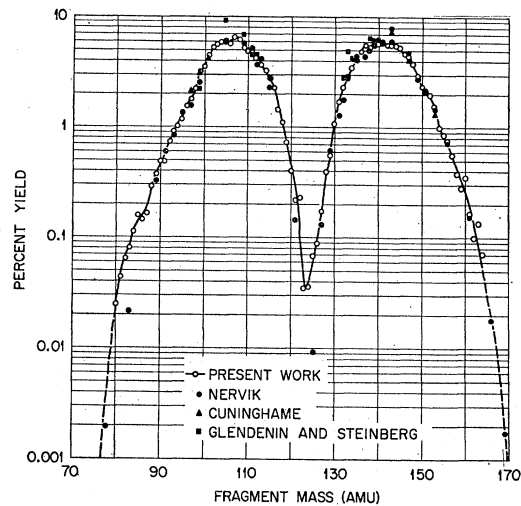

Fig. 7. Post-neutron-emission mass distributions from the present energy, time-of-flight correlation experiment, corrected for experimental resolution. Closed points show the radiochemical data of Nervik (Ref. 14), of Cuninghame (Ref. 15), and of Glendenin and Steinberg (Ref. 16).

tween the results of the present experiment and those of Whetstone[4] are $<0.6\%$; comparison with the "Gaussian fit" results of Fraser et al.[5] shows $\lesssim 1\%$ disagreement, and the slightly lower "direct computation" results of that experiment are consistent with small tailing effects as described in Ref. 5.

The energies and masses tabulated are pre-neutron-emission quantities in the case of the double time-of-flight experiments[4,5]; they are post-neutron-emission quantities in the present experiment. It is significant that the average light- and heavy-fragment energies from the present experiment are nearly independent of the velocity measurement. [Only a relatively weak dependence on fragment mass appears in the energy calibration equation, Eq. (2).] In the experiments of Whetstone[4] and Fraser et al.,[5] the energies are computed from the results of double velocity measurements. The agree-

Fig. 6. Average fragment kinetic energy as a function of fragment mass. The data of Whetstone are from Ref. 4.

TABLE I. Mean values and rms widths of the distributions.

a	This work[b] Direct computation	Whetstone[c] Direct computation	Whetstone[c] Gaussian fit	Fraser et al.[d] Direct computation	Fraser et al.[d] Gaussian fit
E_L (MeV)	103.77 ±0.5 (105.7)[e]	105.71 ±1.06	106.16 ±1.06	104.4±1.0	105.7
σ_{EL} (MeV)	5.48	5.86	5.66	7.5	5.58
E_H (MeV)	79.37 ±0.5 (80.3)[e]	80.01 ±0.80	80.55 ±0.81	78.3±0.7	79.6
σ_{EH} (MeV)	8.23	8.53	8.62	9.5	8.87
V_L (cm/nsec)	1.383±0.006	1.375±0.007	1.372±0.007	1.364	1.370
σ_{VL} (cm/nsec)	0.0693	0.0665	0.063	0.084	0.065
V_H (cm/nsec)	1.036±0.005	1.036±0.005	1.041±0.005	1.023	1.034
σ_{VH} (cm/nsec)	0.0831	0.0795	0.075	0.087	0.077
M_L (amu)	106.0[f]	108.39		107.8	
M_H (amu)	141.9[f]	143.61		144.2	
σ_{ML} (amu)	6.53				
σ_{MH} (amu)	6.55	6.77		7.27	

[a] Subscript L refers to the light fragment, subscript H to the heavy fragment.
[b] Post-neutron emission quantities. The uncertainties given include those in the absolute values; statistical uncertainties are small.
[c] Pre-neutron-emission quantities, Ref. 4.
[d] Pre-neutron-emission quantities, Ref. 5. These authors suggest that their "Gaussian fit" numbers give the better indications of the averages and should be used for comparison with other experiments.
[e] Values in parentheses are pre-neutron-emission energies calculated from the equation $E_{L,H}* = E_{L,H}(1 + \nu_{L,H}/M_{L,H})$.
[f] Uncertainties in the absolute average masses are difficult to evaluate, but are estimated to be $\sim \pm 0.4$ amu. These masses are lower than the pre-neutron masses by ν_L and ν_H, respectively, within these limits.

ment between those energies and the present ones, corrected for neutron emission and given in parentheses, is well within the experimental uncertainties. This agreement, together with the agreement in velocities indicates that the absolute calibrations with heavy ions, together with the present energy calibration procedure, are consistent with the double time-of-flight calibrations based on absolute delay-time measurements.

The post-neutron emission mass distribution of ^{252}Cf obtained from the present experiment and corrected for resolution[13] is shown in Fig. 7 and is tabulated in Table II. Results of the radiochemical measurements of Nervik,[14] of Cuninghame,[15] and of Glendenin and Steinberg[16] are shown in the figure for comparison. There are a few individual points at which discrepancies appear; however, the general agreement with the radiochemical yields is excellent and gives added confidence in the method of energy calibration for the surface barrier detector.

---

[13] The correction for resolution was made according to the equation $N_c(M) = N_u(M) - (\sigma^2/2)[d^2N_c(M)/dM^2]$, where $N_c(M)$ and $N_u(M)$ are the corrected and uncorrected mass distributions, respectively, and σ is the rms width associated with the known (see Ref. 1) mass resolution of ~ 2.5 percent, full width at half-maximum. The second derivative may be evaluated initially at each point in the uncorrected distribution; an iteration procedure (seldom requiring more than one iteration) may then be carried out to obtain $N_c(M)$. J. Terrell (private communication) has pointed out that the most nearly correct result is obtained by averaging the results of the first and second iterations. To obtain the second derivative at each point M and to avoid magnifying statistical fluctuations in the data, we fitted (by least-squares) five points of the distribution to a second-degree polynomial, the center point in each case being the point of interest. It has been shown by Terrell that this method for removing dispersion is essentially equivalent to the three-element operator method previously discussed by him (Ref. 18); the principal difference is that in the present method there is included an analytical procedure for minimizing statistical fluctuations in the distribution.
[14] W. E. Nervik, Phys. Rev. 119, 1685 (1960).
[15] J. G. Cuninghame, J. Inorg. Nucl. Chem. 6, 181 (1948).
[16] L. E. Glendenin and E. P. Steinberg, J. Inorg. Nucl. Chem. 1, 45 (1955).

In the post-neutron-emission mass distribution, fine structure appears which is not completely evident in Fig. 7. Thus we show comparison of the post-neutron-emission mass distribution of Whetstone[4] on a linear plot in Fig. 8. In order not to perturb the original appearance of the structure, neither of these curves has been corrected for resolution. The similarity of shape between the two curves is evident. Most striking, how-

TABLE II. Post-neutron-emission mass yields for ^{252}Cf spontaneous fission fragments, from correlated energy and time-of-flight measurements. The yields have been corrected for experimental resolution. (See text.)

| Mass	Percent yield	Mass	Percent yield	Mass	Percent yield
82	0.064	110	4.971	138	5.266
83	0.082	111	4.931	139	5.564
84	0.115	112	4.327	140	5.806
85	0.156	113	3.805	141	5.859
86	0.148	114	3.265	142	5.621
87	0.163	115	2.810	143	5.685
88	0.281	116	2.191	144	5.590
89	0.372	117	1.419	145	5.196
90	0.487	118	1.123	146	4.612
91	0.477	119	0.731	147	4.471
92	0.727	120	0.404	148	3.744
93	0.911	121	0.216	149	2.751
94	1.029	122	0.226	150	2.384
95	1.219	123	0.035	151	2.107
96	1.535	124	0.036	152	1.936
97	1.747	125	0.068	153	1.510
98	2.229	126	0.088	154	1.007
99	3.098	127	0.171	155	0.868
100	3.490	128	0.393	156	0.758
101	4.394	129	0.557	157	0.559
102	5.414	130	1.081	158	0.389
103	5.556	131	1.718	159	0.283
104	5.916	132	2.329	160	0.359
105	5.935	133	2.843	161	0.167
106	5.742	134	3.493	162	0.100
107	6.536	135	4.031	163	0.137
108	6.215	136	4.953	164	0.070
109	5.348	137	5.465		
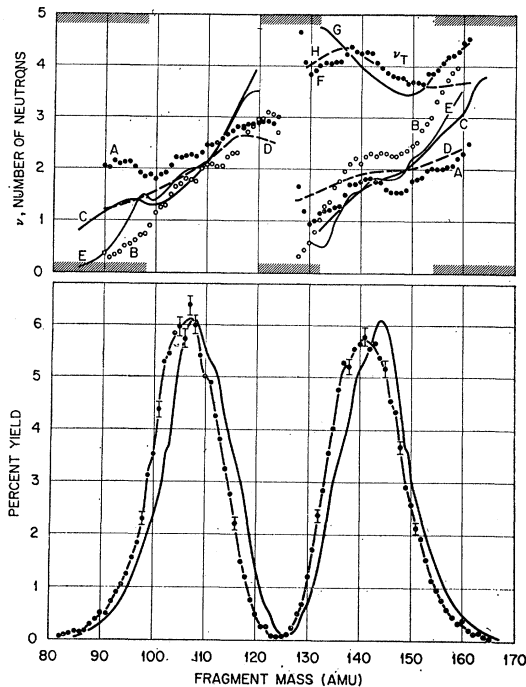
FIG. 8. Mass distributions and number of neutrons $\nu(M^*)$, and $\nu_T(M^*)$. In the lower part of the figure the present post-neutron-emission mass distribution is shown (points and curve) in comparison with the pre-neutron-emission mass distribution (smooth curve) of Whetstone (Ref. 4). Neither curve is corrected for resolution. The upper part of the figure shows $\nu(M^*)$ from cumulative yield calculations in which the present, resolution-corrected mass distribution was used in combination with the resolution-corrected distributions of Whetstone (Ref. 4), curve A, and of Fraser et al. (Ref. 5), curve B. Curves C and D show the results of neutron counting experiments of Bowman et al. (Ref. 7) and Whetstone (Ref. 19), respectively. Curve D is not corrected for resolution effects. Curve E shows the results of Terrell's earlier cumulative yield calculations (Ref. 18). The total number of neutrons ν_T for both fragments, obtained respectively from curves A, C, and D, is plotted as a function of heavy fragment mass in curves F, G, and H. See text.

ever, is the fact that each of the fine structure peaks which appears in the pre-neutron-emission distribution also appears in the post-neutron-emission distribution, displaced to slightly lower masses. The only significant difference in shape between the two curves occurs in the 134-to-145 amu mass range and is easily explained by the rapid change in ν, the number of neutrons emitted, as a function of mass in this mass region.

From this comparison of mass distributions it may be stated that the fine structure in the post-neutron-emission mass distribution reflects only that which appears in the pre-neutron distribution. No significant additional fine structure appears to be introduced by neutron emission, at least within the $\sim 2.5\%$ mass resolution of this experiment. The subject of fine structure in the pre-neutron-emission mass distribution has been discussed by Thomas and Vandenbosch[17] and by Fraser and Milton.[5] These authors have shown that the

[17] T. D. Thomas and R. Vandenbosch, Phys. Rev. 133, B976 (1964).

fine structure peaks are correlated with the even-even parabolas in the function $Q = \epsilon(^{252}\text{Cf}) - \epsilon(Z_L, M^*) - \epsilon(Z_H, A - M^*)$. Here Q is the total energy available for division of the ^{252}Cf nucleus into the two primary fragments of charge and mass Z_L, M^* and $Z_H, A - M^*$, respectively, and ϵ is mass excess in MeV. Results of the present experiment show that the neutron emission properties of the primary fragments are such that similar structure appears in the post-neutron-emission mass distribution.

The average number of neutrons emitted $\nu(M^*)$ may be calculated as a function of primary fragment mass from the two mass distributions by the method of cumulative yields described by Terrell.[18] For this calculation, the resolution-corrected mass distributions were used. The results are shown as closed circles (points labeled A) in the upper part of Fig. 8. The results of the direct neutron counting experiments of Bowman et al.[7] (curve C) and Whetstone[19] (curve D) are shown for comparison. It is gratifying to see that over most of the mass range, i.e., in the regions of the peaks of the mass yield curves, the same trend in $\nu(M^*)$ is followed in both the calculated and measured curves, and the same qualitative structural features are present. Even the disagreement in absolute value of $\nu(M^*)$ does not exceed ~ 0.5 amu in these regions and is generally compensated in the light and heavy groups to give quite good agreement (within ~ 0.3 amu) in the average total number of neutrons emitted by both fragments. This total number of neutrons $\nu_T(M^*)$, is plotted as a function of heavy-fragment mass in the upper part of Fig. 8; the points labeled F were obtained from the $\nu(M^*)$ points labeled (A), and the curves G and H were obtained from the $\nu(M^*)$ curves C and D, respectively. When reading the $\nu(M^*)$ and $\nu_T(M^*)$ curves, note that the mass scale refers to pre-neutron-emission masses.

The cumulative yield calculations for $\nu(M^*)$ in the wings and valley of the mass distribution, i.e., in the mass regions $M \lesssim 98$, $120 \lesssim M \lesssim 132$, and $M \gtrsim 154$, are very sensitive to the accuracy and details of the mass resolution corrections and to small, otherwise negligible experimental effects. A cumulative yield calculation of $\nu(M^*)$ was made from the present, resolution-corrected, post-neutron-emission mass distribution in conjunction with the corrected pre-neutron-emission mass distribution given by Fraser et al.[5] The latter distribution differs very little from that of Whetstone, although slightly higher abundances are given in the wings and valley of their distribution (in the mass regions above). The effect of these slightly higher abundances, probably caused by very small tailing effects as discussed by the authors,[5] is enormously magnified in the $\nu(M^*)$ calculation. Curve B in Fig. 8 shows the results of this calculation. Again the general structural features are preserved (except at $M \sim 100$ amu), and agreement with the direct

[18] J. Terrell, Phys. Rev. 127, 880 (1962).
[19] S. L. Whetstone, Jr., Phys. Rev. 114, 581 (1959).

measurements is within ~0.5 amu for masses near the peaks of the distribution. As in the first calculation, however, the discrepancies are large in the wings; they are opposite in direction from those appearing in the case of the first calculation (curve A). A comparison of curves A and B shows the rather large change in the calculated function $\nu(M^*)$, especially in the wings, resulting from relatively small changes in the pre-neutron-emission mass distribution. For reference we have included the results of Terrell's cumulative yield calculation[18] based on earlier double time-of-flight data for pre-neutron-emission masses and on radiochemical data for the post-neutron-emission masses.

The uncertainties in $\nu(M^*)$ as calculated from mass distributions appear to arise almost entirely from small uncertainties in the mass distributions themselves, particularly in the wings and valley. Thus the ranges of validity of the $\nu(M^*)$ calculations in the present work (curves A and B) are limited to the regions $98 \lesssim M \lesssim 120$ and $132 \lesssim M \lesssim 154$. The differences between curves A and B in these regions is probably a good measure of the uncertainty in such cumulative yield determinations of $\nu(M^*)$.

ACKNOWLEDGMENTS

The authors are especially grateful to S. G. Thompson for supplying the ^{252}Cf source and to C. D. Moak for his help in the heavy-ion work. The assistance of Mary M. Kedl in carrying out the computer calculations and the technical assistance of D. G. Peach throughout this work are gratefully acknowledged. The authors are grateful to J. S. Fraser, W. M. Gibson, J. C. D. Milton, J. Terrell, and T. D. Thomas for helpful discussions and suggestions. One of us (W.E.K.) is pleased to acknowledge the support of an Oak Ridge Institute of Nuclear Studies Graduate Fellowship.

APPENDIX I

Determination of Absolute Ion Energies

Absolute energy and velocity calibrations for the system may be made, once the energies and velocities of the ions emerging from the analyzing magnet are known. In order to know these quantities, it is necessary first to identify the ion charge associated with each peak in the pulse-height or time-of-flight spectrum. The ion charge for each peak may be identified easily from measurements at two magnetic fields corresponding to two resonance frequencies in a nuclear magnetic resonance fluxmeter. Energy, mass, and charge of the ion and the fluxmeter frequency f are related by the equation

$$ME/q^2 = kf^2, \qquad (A1)$$

where E is the kinetic energy in MeV, M is the exact mass of the ion in amu, q is the charge number, i.e., the number of electrons missing from the neutral atom, and k is the calibration constant of the magnet. The relativistic correction for Eq. (A1) is negligible.
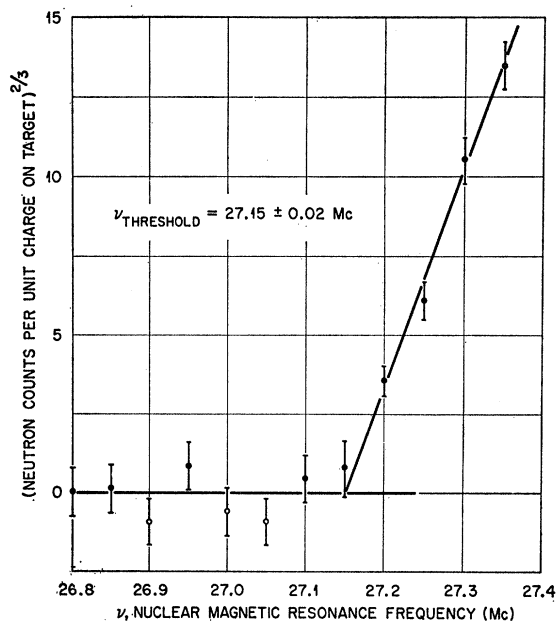

FIG. 9. Threshold determination for $D(^{16}O,n)^{17}F$ reaction. Oxygen O^+ beam; threshold energy 14.548 MeV.

The method for identification of ion charge states q is discussed in detail in Ref. 8 and will not be repeated here. The method does not require that the value of k be known; thus charge assignments may be made without reference to the ion energies. The absolute ion energy assignments, on the other hand, depend directly on k as indicated in Eq. (A1). Therefore an accurate determination of k was made from $D(^{16}O,n)^{17}F$ threshold measurements. The Q value for this reaction is taken to be 1.627 MeV[20]; the corresponding ^{16}O threshold energy is 14.548 MeV.

A standard long counter was placed at 0° with respect to the ^{16}O beam, and neutron counts were obtained as a function of f. Both the oxygen 3+ and 4+ beams were used; the target was a newly fabricated Zr-D platinum backed target. Background counts were obtained with the beam incident on a blank target; the background counts were generally low. Several such runs were made; results of a typical run are shown in Fig. 9. The oxygen 4+ beam was used in this case, and as is standard in threshold determinations, the two-thirds power of the background-corrected count rate is plotted as a function of magnetic resonance frequency. The results of this run, averaged with those of the corresponding oxygen 3+ run, gave

$$k = 0.01974 \pm 0.00001 \, (\text{MeV}) \, (\text{amu}) / (\text{Mc/sec})^2 (e)^2,$$

where e is the unit of ion charge (an integer). This value is in excellent agreement with earlier values obtained[21]

[20] T. Lauritsen and F. Ajzenberg-Selove, *Nuclear Data Sheets*, compiled by K. Way *et al.* (Printing and Publishing Office, National Academy of Sciences–National Research Council, Washington, D. C., 1962).
[21] C. D. Moak and G. F. Wells (private communication).

from nuclear-level and reaction-threshold determinations with light bombarding particles at lower magnetic fields. Thus differential hysteresis effects were negligible.

Some of the heavy-ion measurements were made at magnetic fields higher than those corresponding to the threshold measurements. In these cases, however, the pulse-height spectra were carefully followed in a series of measurements from the lower to the higher fields. Again no differential hysteresis effects were found. The absolute energies assigned to the heavy-ion peaks in all spectra are accurate to about $\pm 0.2\%$.

APPENDIX II

Extensive studies[9] of the response of a wide variety of surface barrier and diffused junction detectors to heavy ions and fission fragments, together with the work reported in this paper, suggest that an equation of the form of Eq. (2) in the text (and repeated below) might apply in general for the calibration of solid-state detectors for heavy ions and fission fragments. Accordingly, we have developed a method for obtaining precise values of the constants in the equation simply from a pulse-height spectrum of ^{252}Cf spontaneous fission fragments. For this purpose the fragments must be unperturbed (e.g., by passage through a backing foil), but otherwise there are no special requirements. (See last paragraph, however.)

Let us repeat Eq. (2) here for reference:

$$E = (a + a'M)x + b + b'M. \qquad (A2)$$

Here E and M are the ion energy and mass, respectively, and x is the corresponding pulse height. For a given detector in the present studies, the constants a, a', b, and b' may be determined directly from pulse-height-versus-energy data for Br and I, such as that shown in the top part of Fig. 10. The alpha-particle curve in the figure is shown only for comparison and will not be used in any of this development.

The ^{252}Cf pulse-height spectrum, shown in the lower part of the figure, was obtained under the same conditions as the Br and I data, and in the same sequence of runs. Extreme care was exercised in maintaining low amplifier noise, constant system gains, etc., throughout these runs. The intercalibrations and checks on stability and linearity were carried out as discussed in the text.

The ^{252}Cf spectrum is used to define two pulse heights which we will call P_L and P_H. The pulse height P_L corresponds to the midpoint between the $\frac{3}{4}$-maximum points in the light-fragment peak; the pulse height P_H corresponds to the midpoint between the $\frac{3}{4}$-maximum points in the heavy-fragment peak.

As shown in the figure the Br and I energies corresponding to each pulse height may be determined. We designate the Br and I energies corresponding to the pulse height P_L as $E_{L,80}$ and $E_{L,127}$, respectively; the energies corresponding to P_H are similarly designated $E_{H,80}$ and $E_{H,127}$. These four energies should be "uni-
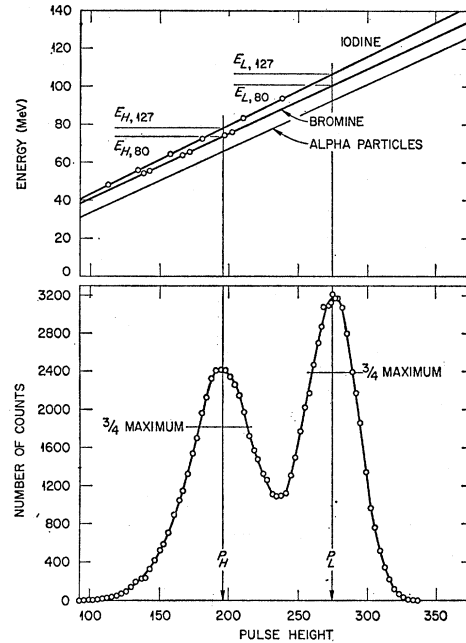

FIG. 10. Energy calibration of solid-state detectors for heavy ions and fission fragments. The upper part of the figure shows the energy versus pulse height relations for Br and I ions, and alpha particles. The corresponding pulse-height spectrum for ^{252}Cf fission fragments is shown below.

versal" constants for detectors not differing too much from those used in this work.

Three different surface barrier detectors were used in separate sets of measurements to determine these energies; the window thicknesses (gold) ranged from 30 to 75 μg/sq cm. The individual values thus obtained (three for each energy) agreed within ± 0.15 MeV. The results for each energy were averaged, and the following values were obtained:

$$
\begin{aligned}
E_{L,80} &= 100.57 \text{ MeV}, \\
E_{L,127} &= 107.01 \text{ MeV}, \\
E_{H,80} &= 73.69 \text{ MeV}, \\
E_{H,127} &= 78.45 \text{ MeV}.
\end{aligned}
\qquad (A3)
$$

Evaluation of all of the uncertainties indicates that uncertainties of about $\pm 0.3\%$ (standard deviation) are associated with the values of Eq. (A3).

The energies given in Eq. (A3) may now be used in conjunction with the values of P_L and P_H obtained in any experiment to set up four simultaneous equations from which the four constants in Eq. (A2) may be precisely determined. For convenience in application we write here the solutions in terms of P_L and P_H:

$$
\begin{aligned}
a &= 24.0203/(P_L - P_H), \\
a' &= 0.03574/(P_L - P_H), \\
b &= 89.6083 - aP_L, \\
b' &= 0.1370 - a'P_L.
\end{aligned}
\qquad (A4)
$$

It has been suggested that the general procedure outlined above may be used more practically by some experimenters with points of reference in the [252]Cf spectrum other than the midpoints at $\frac{3}{4}$-maximum. (For example, Gaussian fits may be made over the peaks of the distribution and the most probable points could be used.) Accordingly we include a tabulation of a [252]Cf pulse-height spectrum in Table III, which together with the following calibration equation allows the choice of any reference points. The appropriate calibration equation for the pulse-height spectrum of Table III is

$$E= (0.8266+0.001230M)x+3.3051+0.00860M. \quad (A5)$$

In the case of diffused junction detectors, evidence[9,22] indicates that the above calibration procedure may be used, as long as the window is not too thick. In the case of either surface barrier or diffused junction detectors, the following notes of caution are important:

(1) The detector must be operated in the saturation region of the pulse-height-versus-bias curve. The linear dependences observed in the pulse-height-versus-energy relation, including the mass dependence, may result from fortuitous relations between the energy loss of heavy ions in the thin gold layer and the "charge collection" efficiency in the sensitive volume, both of which are functions of the ion mass and energy. Tests of the above calibration procedure have not been made for detector biases ouside of the saturation region.

(2) Application of this method of calibration may not be valid in those experiments where the particle masses and/or energies are outside the mass and energy regions associated with fission fragments. No tests have been made for particle masses and energies outside these regions.

(3) Undesirable experimental effects giving rise to spectrum distortion should be avoided. Such effects include charge multiplication in the detector,[23] radiation damage in the detector,[24] and improper pulse formation in the detector or charge-sensitive amplifier.

In some experiments in which fragments pass through a backing foil, e.g., energy correlation experiments, it

[22] W. M. Gibson and T. D. Thomas (private communication).
[23] F. J. Walter, IEEE Trans. Nucl. Sci. NS-11, No. 3, 232 (1964).
[24] H. C. Britt and G. C. Benson, Rev. Sci. Instr. (to be published)

TABLE III. Pulse-height spectrum for [252]Cf spontaneous fission fragments, for reference in the energy calibration of solid-state detectors.

Ch. No. x	Counts	Ch. No. x	Counts	Ch. No. x	Counts
50	472	74	9679	98	8678
51	580	75	9646	99	9615
52	690	76	9790	100	10 420
53	807	77	9621	101	11 144
54	994	78	9270	102	12 014
55	1104	79	8893	103	12 410
56	1376	80	8428	104	12 791
57	1598	81	7848	105	12 904
58	1835	82	7101	106	12 750
59	2200	83	6592	107	12 211
60	2534	84	6197	108	11 487
61	2967	85	5475	109	10 379
62	3387	86	5128	110	9432
63	3811	87	4966	111	8272
64	4347	88	4595	112	7155
65	4814	89	4669	113	5871
66	5502	90	4522	114	4721
67	5988	91	4416	115	3629
68	6663	92	4696	116	2877
69	7346	93	5020	117	2092
70	7856	94	5684	118	1453
71	8389	95	6210	119	1002
72	8892	96	6984	120	681
73	9473	97	7716	121	427

may be desirable to include a correction for energy loss in the foil directly in the calibration constants. This may be accomplished in either of two ways: (a) Fragments from [252]Cf fission may be allowed to pass through the backing foil and into the detector of the experiment. The [252]Cf spectrum thus obtained may be treated as described above and the appropriate calibration constants obtained. (b) If two points may be uniquely identified in the pulse-height spectrum for the fragments under study, one may use the calibration constants a, a', b, b' obtained from a [252]Cf spectrum (fragments not perturbed by foil) to derive a new set of four energies corresponding to two masses and to the two pulse heights chosen in the unperturbed fragment spectrum under study. The source (or target) may now be rotated through 180°, and a similar spectrum obtained for the fragments passing through the foil. Assignment of the new energies (and masses) to the appropriate pulse heights in this spectrum, with the solution of the four simultaneous equations, will yield the desired calibration constants.